BULLETIN OF THE EARTHQUAKE
RESEARCH INSTITUTE
Vol. 37 (1959), pp. 53-87

5. *Comparative Studies of Earthquake Motions on the Ground and Underground. (Multiple Reflection Problem).*

By Kiyoshi KANAI, Teiji TANAKA and Shizuyo YOSHIZAWA,

Earthquake Research Institute.

(Read Dec. 17, 1957 and May 27, 1958.—Received Dec. 28, 1958.)

Summary

A spectral analysis of seismograms obtained both on the ground and underground has been carried out. The observation places were at Hitachi Mine and Tokai-mura, Ibaraki Prefecture.

It was clarified by comparing the observational results with the theoretical results, that the amplitude on the ground grows very large according to the multiple reflection of seismic waves in the superficial layer.

1. Introduction

It has been proved by many authors[1] that the amplitudes of earthquake motions underground are smaller than the one on the ground and the shorter the period of earthquake is, the smaller the ratio of the amplitudes underground to the one on the ground. Recently, the following points were clarified from the results of comparative observations made at Hitachi Mine, Ibaraki Prefecture, both on the ground and in the depth of the ground.

(i) The distribution of the horizontal component of seismic waves as to the depth in the earth is not so simple as considered formerly, and the component takes the maximum or the minimum amplitudes of waves at a certain depth like 150 meters underground in general[2].

(ii) In cases where the period of the seismic waves at a great

1) J. MILNE, *Trans. Seism. Soc.*, **10**.
S. SEKIYA and F. OMORI, *Trans. Seism. Soc.*, **16** (1892).
S. T. NAKAMURA, *Proc. Physico-Mathem. Soc. Japan*, **7** (1925), 127.
N. NASU, *Bull. Earthq. Res. Inst.*, **9** (1931), 454.
W. INOUE, *Bull. Earthq. Res. Inst.*, **12** (1934), 712.

2) K. KANAI and T. TANAKA, *Bull. Earthq. Res. Inst.*, **29** (1951), 107-113.

depth coincides with the peak period of the period-frequency curve on the surface which corresponds to the natural period of surface layer, the amplitude at the surface of the ground grows very large. But, when the successive waves of the same period are few, the surface layer has little influence upon the amplitude on the ground, even if the periods of primary waves may be approximate to the natural period of surface layer[3].

(iii) The peak period of the period-frequency curve of micro-tremor is coincident with the natural period of surface layer in case of *S*-waves[4].

(iv) The relation between the maximum displacement of the spectral response of the seismic waves at the great depth of 100 km epicentral distance, $A_{m.s}$, and the period corresponding to it, T_m, may be written as follows:

$$A_{m.s}=0.053T_m^{2.56}\ ^{5)}$$

The amplitude-period relation of seismic waves at the great depth, excepting those of considerably short and long periods, can be assumed as follows:

$$\frac{2\pi A}{T}(\equiv\text{velocity})=\text{constant.}$$

In the present investigations, firstly, we are going to carry out the spectral analysis[6] of seismograms obtained both on the ground and underground at Hitachi Mine and Tokai-mura, Ibaraki Prefecture. Secondly, mathematical examinations based on the theory of the multiple reflection of seismic waves in the visco-elastic layer will be made of the results of this spectral analysis.

2. The case of Hitachi Mine, Ibaraki Prefecture

The places of comparative observations were on the ground surface 370 meters above sea-level and at a depth of 300 meters from the ground surface.

3) K. KANAI, K. OSADA and S. YOSHIZAWA, *Bull. Earthq. Res. Inst.*, **31** (1953), 227–234.

4) K. KANAI, K. OSADA and S. YOSHIZAWA, *Bull. Earthq. Res. Inst.*, **32** (1954), 361–370.

5) K. KANAI and S. YOSHIZAWA, *Bull. Earthq. Res. Inst.*, **36** (1958), 275–293.

6) R. TAKAHASI, *Proc. 3rd Japan National Congr., Applied Mech.* (1953), 373.

The positions of seismograph stations together with the geological formations of the area and the velocity distribution of *P*-waves in the depth of the same area are shown in Figs. 1 and 2. In Table 1 the

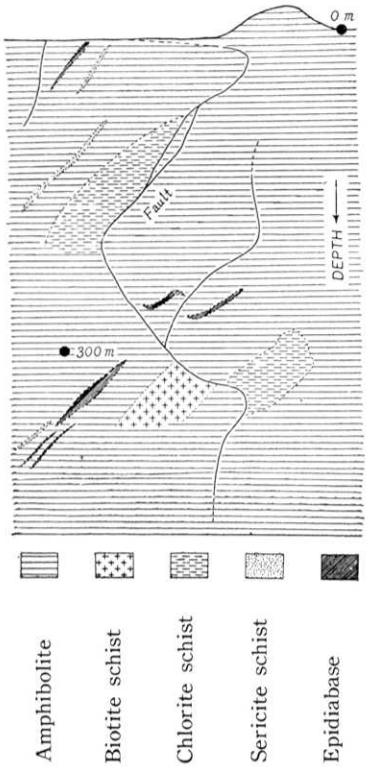

Fig. 1. Geological formations of the neighbouring part of observing stations at Hitachi Mine.

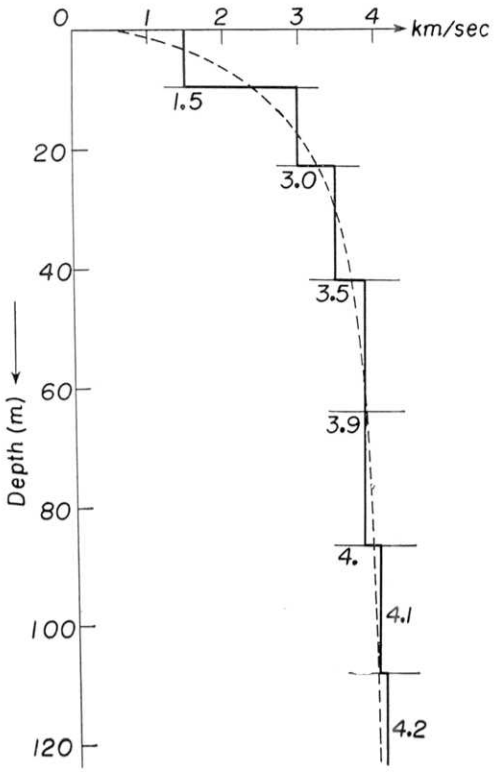

Fig. 2. Velocity of *P*-waves versus depth from the earth's surface at Hitachi Mine.

Table 1. Constants of seismographs used at Hitachi Mine.

Position	Observing direction	Natural period in sec	Damping ratio	Magnification
0 m (surface)	E W	1.0	13:1	220, 440
	N S	0.9	13:1	180, 380, 400
−300 m	E W	0.9	13:1	200, 430
	N S	1.0	13:1	465, 430

constants of the seismographs used in the present case are shown. The representative records obtained both on the earth's surface and 300 meters underground are illustrated in Fig. 3.

The observing places and the epicenters treated in this case are shown in Fig. 4. And in Table 2 the number, data and hypocenter of these earthquakes are listed.

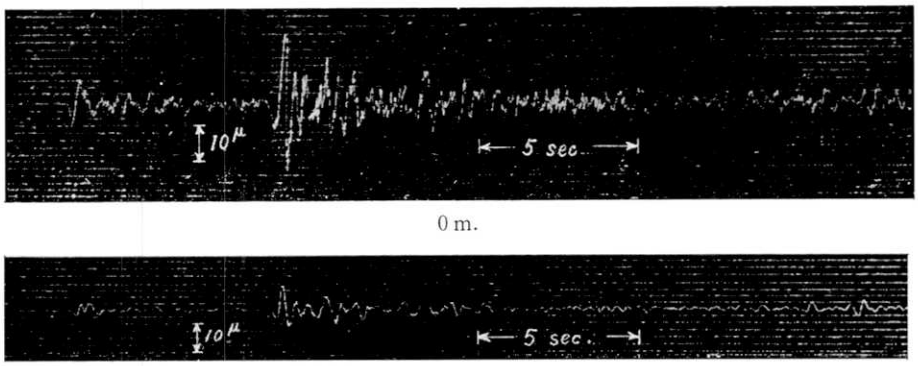

Fig. 3. Representative seismograms obtained at Hitachi Mine.

In the cases of Nos. 797, 828 and 837, newbuilt electric self-starters[7] were used in the recording system and the recording speed was 1 cm

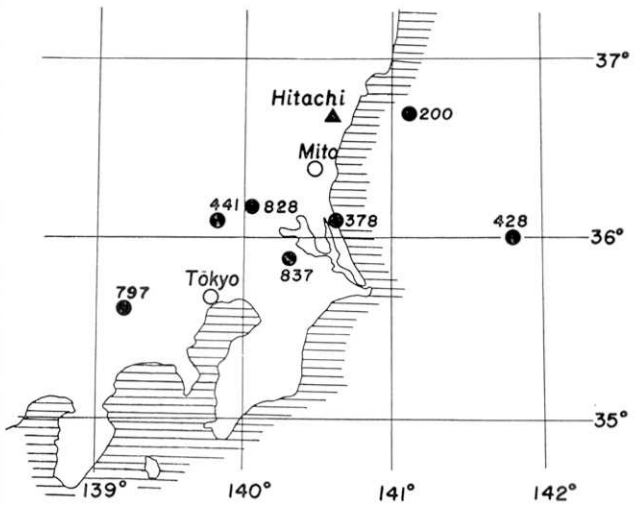

Fig. 4. Epicenters of the earthquakes observed at Hitachi Mine.

7) T. TANAKA, *Bull. Earthq. Res. Inst.*, **36** (1958), 445.

Table 2. Earthquakes observed at Hitachi Mine.

Earthquake No.	Date	Origin			Duration preliminary tremer in sec	Observing direction
		N	E	Depth in km		
200	1952 III 10	36.7	141.1	40	8.0	EW
378	〃 XI 18	36.1	140.6	60	9.9	NS
428	1953 I 14	36.0	141.8	60	14.3	EW
441	〃 〃 26	36.1	139.9	40	9.8	〃
797	1956 XII 19	35.6	139.2	120	—	NS
828	1958 II 8	36.2	140.1	80	—	〃
837	〃 III 17	35.6	140.3	70	—	〃

per sec. In other cases, that is, Nos. 200, 378, 428 and 441, no starter was used and then recording speed was 0.21 cm per sec.

The displacement spectra of the earthquake motions obtained by means of the response computer are shown in Figs. 12～18. The velocity and acceleration spectra have been calculated from the displacement spectra on the assumption of simple harmonic motion. The velocity and acceleration spectra are presented in Figs. 19～25 and 26～32, respectively. Generally speaking, it will be seen from Figs. 12～18 that there is a peak in every displacement-period curve and the larger the maximum displacement is, the longer the period corresponding to it will be. Figs. 19～25 tell us that the velocity-period curve at 300 meters underground, excepting a few cases, takes a considerably flat form. And then, as it

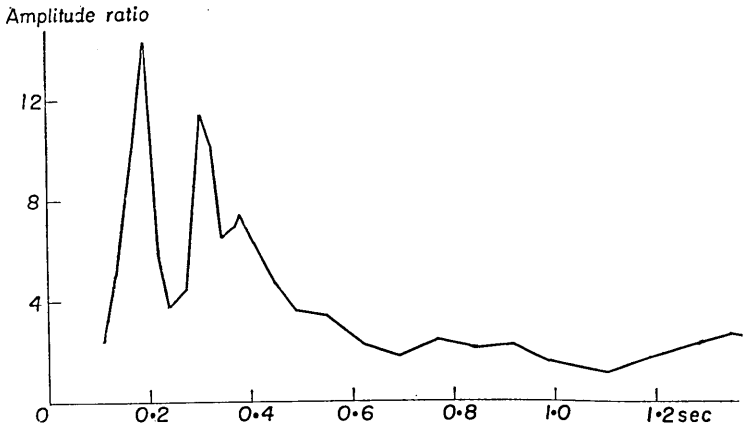

Fig. 5. Amplitude ratio of the ground surface to the 300 m depth at Hitachi Mine. Earthquake number: 200.

can be seen from Figs. 26~32, excepting considerably short periods the shorter the period of earthquake motions at 300 meters depth is, the larger the acceleration will be.

These displacement-, velocity- and acceleration-period relations of earthquake motion have already been examined closely in the previous paper[8].

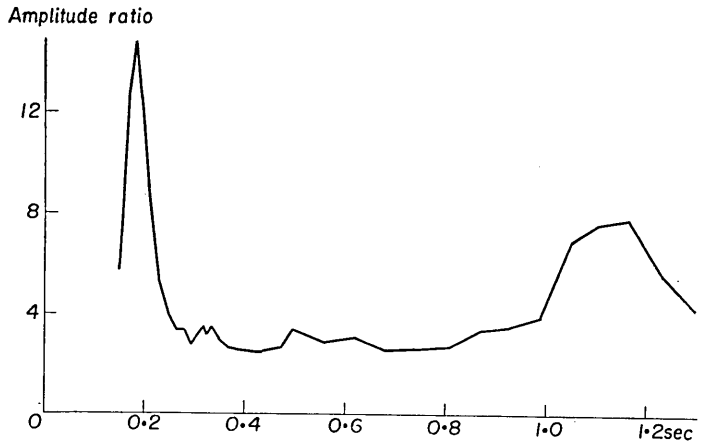

Fig. 6. Amplitude ratio of the ground surface to the 300 m depth at Hitachi Mine. Earthquake number: 378.

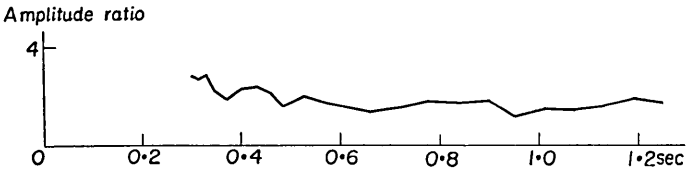

Fig. 7. Amplitude ratio of the ground surface to the 300 m depth at Hitachi Mine. Earthquake number: 428.

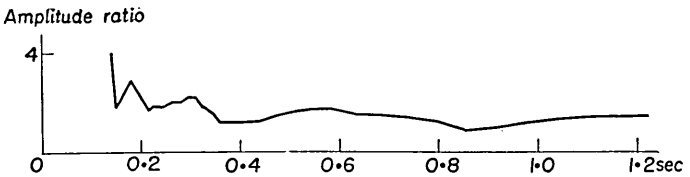

Fig. 8. Amplitude ratio of the ground surface to the 300 m depth at Hitachi Mine. Earthquake number: 441.

8) *loc. cit.*, 5).

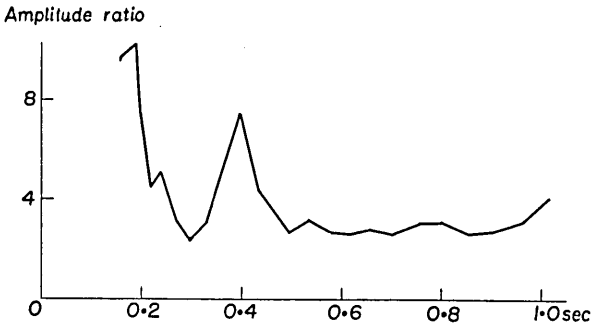

Fig. 9. Amplitude ratio of the ground surface to the 300 m depth at Hitachi Mine. Earthquake number: 797.

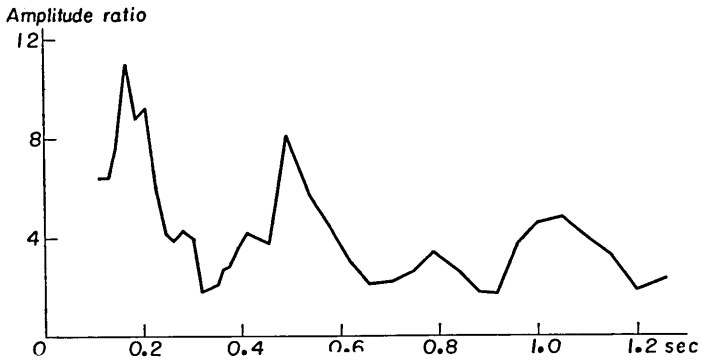

Fig. 10. Amplitude ratio of the ground surface to the 300 m depth at Hitachi Mine. Earthquake number: 828.

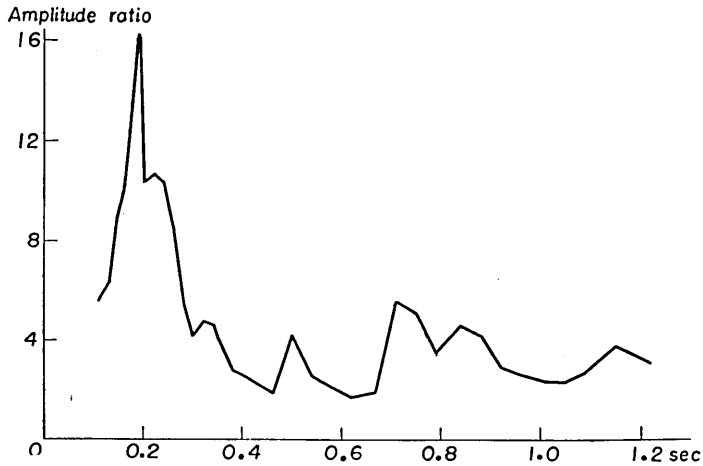

Fig. 11. Amplitude ratio of the ground surface to the 300 m depth at Hitachi Mine. Earthquake number: 837.

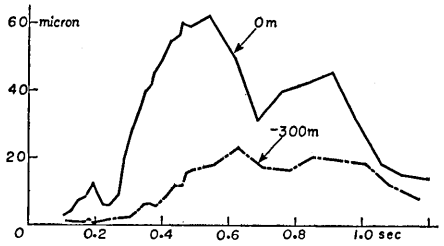

Fig. 12. Displacement spectra of earthquake No. 200 at Hitachi Mine.

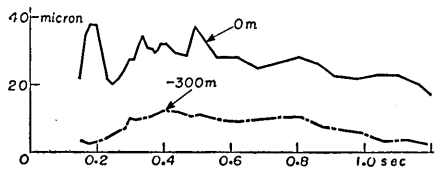

Fig. 13. Displacement spectra of earth quake No. 378 at Hitachi Mine.

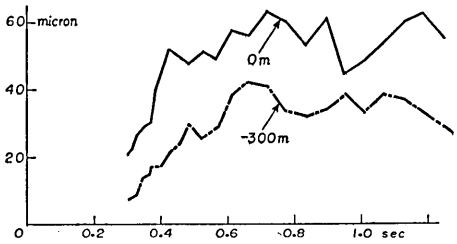

Fig. 14. Displacement spectra of earthquake No. 428 at Hitachi Mine.

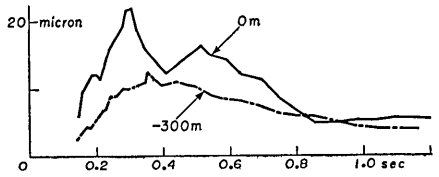

Fig. 15. Displacement spectra of earthquake No. 441 at Hitachi Mine.

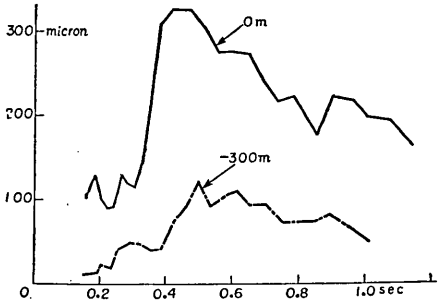

Fig. 16. Displacement spectra of earthquake No. 797 at Hitachi Mine.

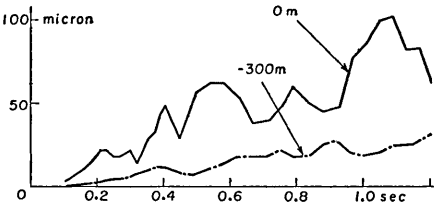

Fig. 17. Displacement spectra of earthquake No. 828 at Hitachi Mine.

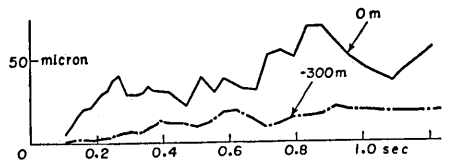

Fig. 18. Displacement spectra of earthquake No. 837 at Hitachi Mine.

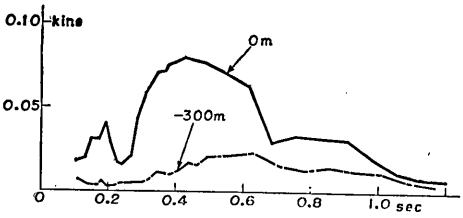

Fig. 19. Velocity spectra of earthquake No. 200 at Hitachi Mine.

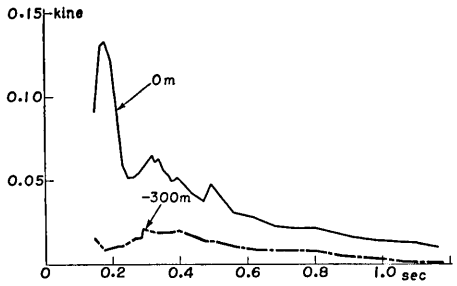

Fig. 20. Velocity spectra of earthquake No. 378 at Hitachi Mine.

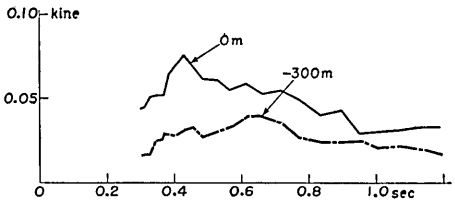

Fig. 21. Velocity spectra of earthquake No. 428 at Hitachi Mine.

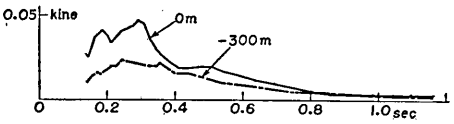

Fig. 22. Velocity spectra of earthquake No. 441 at Hitachi Mine.

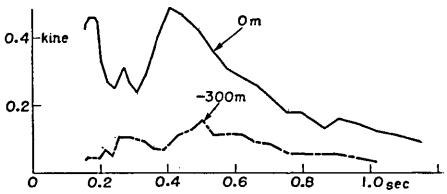

Fig. 23. Velocity spectra of earthquake No. 797 at Hitachi Mine.

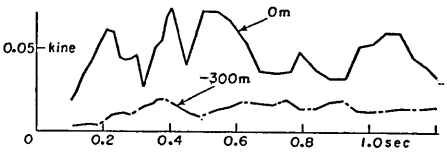

Fig. 24. Velocity spectra of earthquake No. 828 at Hitachi Mine.

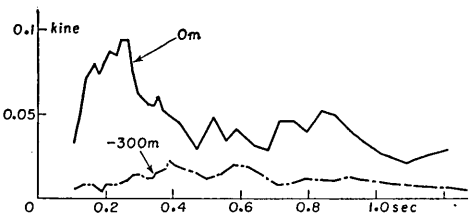

Fig. 25. Velocity spectra of earthquake No. 837 at Hitachi Mine.

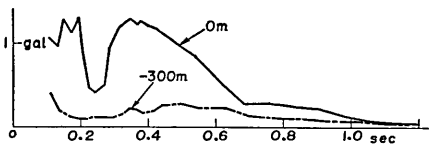

Fig. 26. Acceleration spectra of earthquake No. 200 at Hitachi Mine.

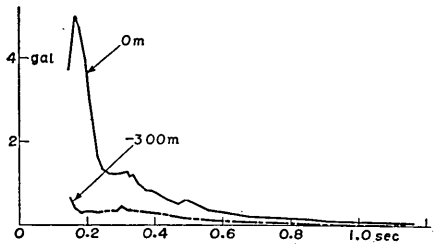

Fig. 27. Acceleration spectra of earthquake No. 378 at Hitachi Mine.

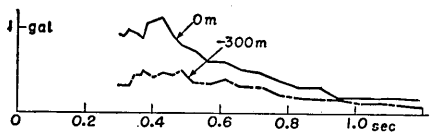

Fig. 28. Acceleration spectra of earthquake No. 428 at Hitachi Mine.

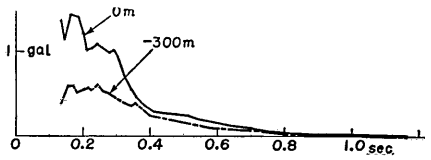

Fig. 29. Acceleration spectra of earthquake No. 441 at Hitachi Mine.

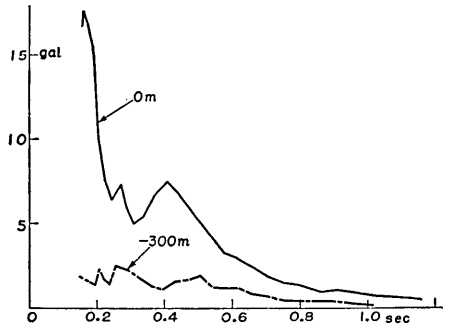

Fig. 30. Acceleration spectra of earthquake No. 797 at Hitachi Mine.

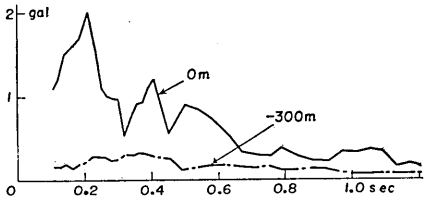

Fig. 31. Acceleration spectra of earthquake No. 828 at Hitachi Mine.

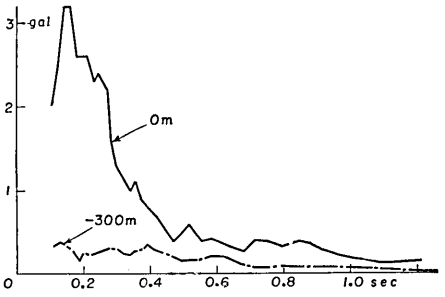

Fig. 32. Acceleration spectra of earthquake No. 837 at Hitachi Mine.

Also, it may be found from Figs. 12～18 that the amplitude of earthquake motion on the ground is larger than that in the depth of the ground in every period. In order to make clearer the amplitude relation between the ground surface and underground, we calculated the amplitude ratio of the ground surface to the underground in each period from the results of spectral analysis which are shown in Figs. 12～18. And then, the relations of the abovementioned ratio to period are shown in Figs. 5～11, which tell us that, in general, the amplitude of earthquake motions on the ground in Hitachi Mine corresponding to the period of 0.18 sec, that is, the predominant period of that place, grews considerably large and the curves in these figures seem to be similar to the amplitude-period curve of a body having a single surface layer. The results of the mathematical studies concerning these features will be described in the next section but one.

3. The case of Tokai-mura, Ibaraki Prefecture

In this case, two comparative observations of earthquake motions at ground surface and underground were made. One was made at the place named (A) in which two horizontal seismographs were installed at the ground surface and 21.1 m underground. Another was made at the place named (B) in which three horizontal seismographs were installed at the ground surface, 7 m and 21.3 m underground. Subsoil conditions detected by boring and observation spots are shown in Fig. 33. In Table 3, 4 the constants of the seismographs used in the present case are shown.

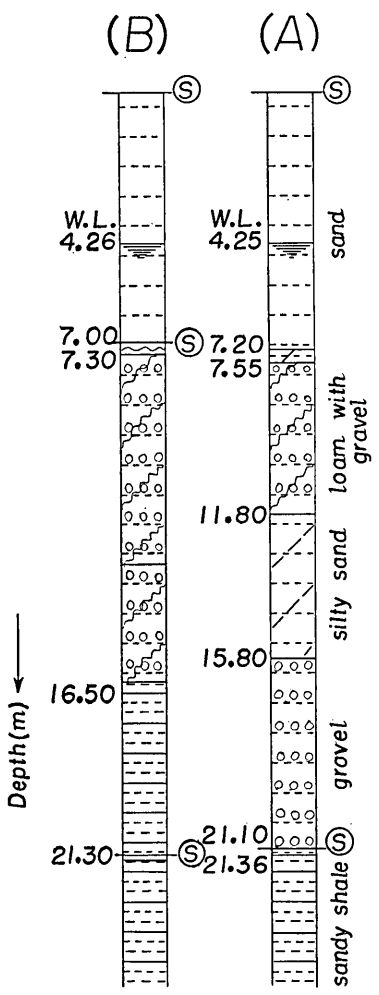

Fig. 33. Subsoil conditions of places (A) and (B) in Tokai-mura as detected by boring.

In the present case, newbuilt electric self-starters were used in the recording system and recording speed was 1 cm per sec. The representative records obtained both on the earth's surface and underground are illustrated in Fig. 34. The observing places and the epicenters treated in this case are shown in Fig. 35. And Tables 5, 6 represent the number, date and hypocenter of these earthquakes.

The displacement spectra of the earthquake motions observed at place (A) in Tokai-mura by means of the response computer are shown in Figs. 36~44. The velocity and acceleration spectra have been calculated from the displacement spectra on the assumption of simple harmonic motion. They are presented in Figs. 45~53 and Figs. 54~62, respectively. It will be seen from Figs. 36~62 that, in general, the displacement-, velocity- and acceleration-period relations of earthquake motions are the same as the results mentioned in the previous paper and also in the preceding chapter.

The ratio of the amplitude on the ground to that underground in

Table 3. Constants of seismographs used at place (A) in Tokai-mura.

Type	Position	Observing direction	Natural period in sec	Damping ratio	Magnification
mechanical	0 m	EW	0.9	13:1	276
		NS	1.0	13:1	278
electro-magnetic	0 m	NS	0.7	critical damping	400
self-levelling	−21.1 m	NS	0.7		600

Table 4. Constants of seismographs used at place (B) in Tokai-mura.

Type	Position	Observing direction	Natural period in sec	Damping ratio	Magnification
mechanical	0 m	EW	0.9	11:1	265
		NS	1.0	8:1	250
self-levelling	− 7.0 m	NS	0.7	critical damping	400
	−21.3 m	NS	0.7		1200 950

each period obtained from Figs. 36～44 are shown in Figs. 63～71 which tell us that, in general, the amplitude of earthquake motions on the ground at place (A) in Tokai-mura corresponding to the period of 0.27 sec, that is, the predominant period of that place, grew considerably large and the curves in these figures seem to be similar to amplitude-period curve of a body having a single surface layer. The mathematical studies will be presented in the next chapter.

The displacement-, velocity- and acceleration-period relations of earthquake motions observed on the ground, 7 m and 21 m underground of place (B) in Tokai-mura are shown in Figs. 72～78, 79～85 and 86～92, respectively. And then, the relation between the ratios of the amplitude on the ground and 7 m underground to the one 21 m underground and period are shown in Figs. 93～99. In the present case, as seen in Figs. 93～99, the relation between the amplitude ratio mentioned above and period seems to be somewhat complex in comparison with the for-

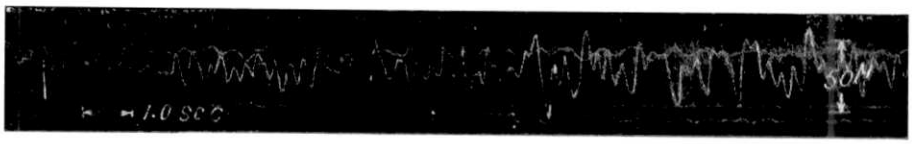

0 m at place (A).

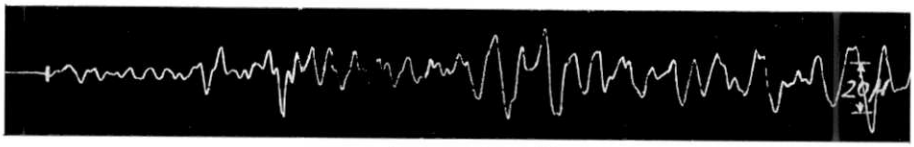

−21 m at place (A).

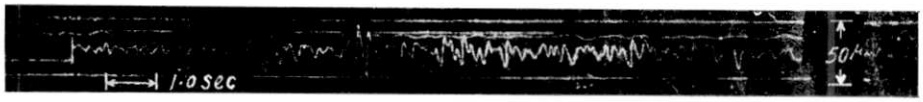

0 m at place (B).

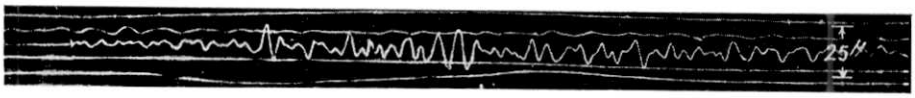

−7 m at place (B).

−21 m at place (B).

Fig. 34. Representative seismograms observed at Tokai-mura.

mer cases, that is, the cases at Hitachi Mine and place (A) in Tokai-mura.

In general, in cases when the earthquake origin is in the sea, the vibration characteristics of short period of ground scarcely appear because it seems that the amplitude of short period of earthquake motions is too small in the case of the sea earthquake.

Otherwise, Figs. 72∼92, especially velocity-period relation of Figs. 80∼83, tell us that the amplitude of earthquake motions on the ground at place (B) in Tokai-mura corresponding to the period of 0.24 sec, that is, the predominant period of that place, grew considerably large. The mathematical treatment of this problem will be dealt with in the next chapter.

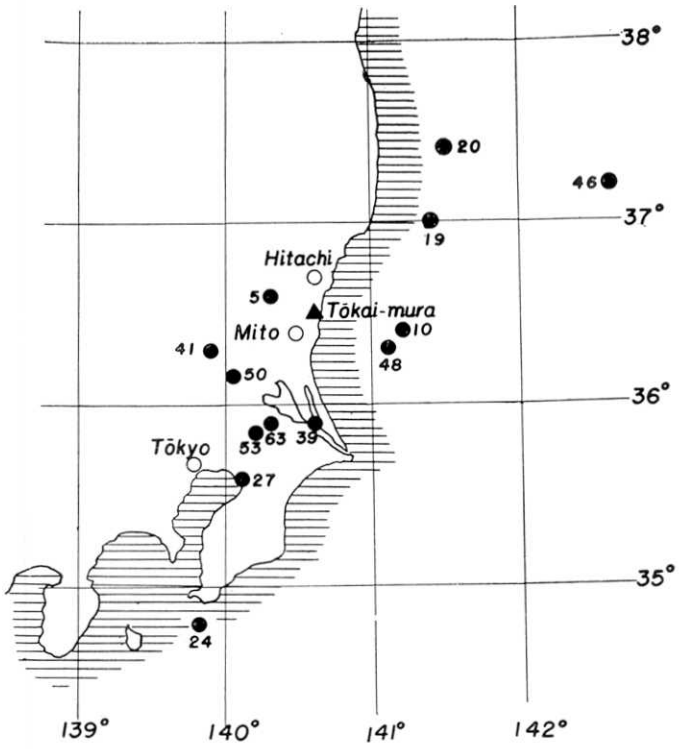

Fig. 35. Epicenters of earthquakes observed at Tokai-mura.

Table 5. Earthquakes observed at place (A) in Tokai-mura.

Earthquake No.	Date	Origin		
		N	E	Depth in km
39	1957 XII 27	35.9	140.6	about 40
41	1958 I 22	36.3	139.9	80
46	〃 〃 29	37.1	142.6	60
48	〃 II 5	36.3	141.1	40
50	〃 〃 8	36.2	140.1	80
53	〃 〃 18	35.9	140.2	60
63	〃 III 17	35.9	140.3	70

Table 6. Earthquakes observed at place (B) in Tokai-mura.

Earthquake No.	Date	Origin		
		N	E	Depth in km
3	1957 VII 26	Off E coast of Ibaraki Prefecture		
5	〃 VIII 2	36.6	140.3	110
10	〃 〃 7	36.4	141.2	shallow
19	〃 〃 18	37.0	141.4	about 60
20	〃 〃 31	37.4	141.5	about 30
24	〃 IX 7	34.8	139.8	about 90
27	〃 X 4	35.6	140.1	about 60

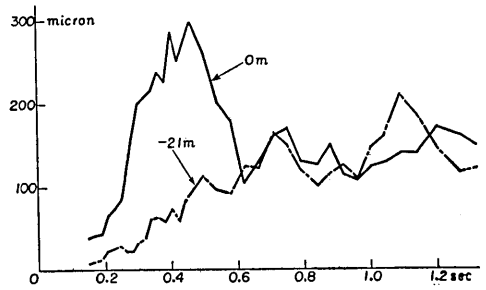

Fig. 36. Displacement spectra of earthquake No. 39 at place (A) in Tokai-mura.

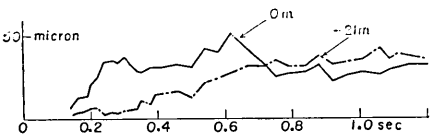

Fig. 37. Displacement spectra of earthquake No. 41 at place (A) in Tokai-mura

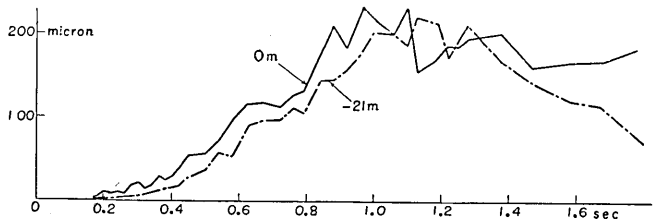

Fig. 38. Displacement spectra of earthquake No. 46 at place (A) in Tokai-mura.

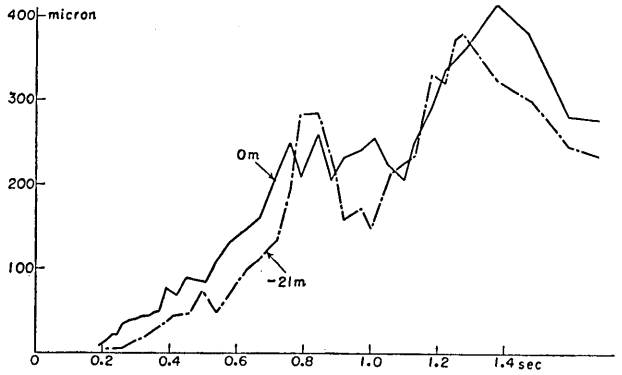

Fig. 39. Displacement spectra of earthquake No. 50 at place (A) in Tokai-mura.

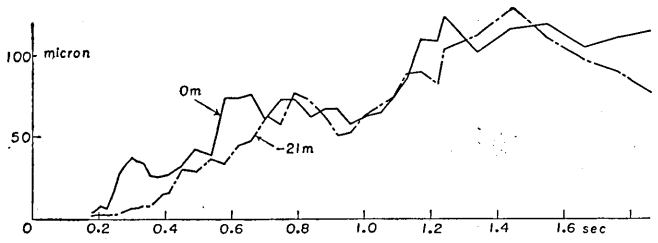

Fig. 40. Displacement spectra of earthquake No. 53 at place (A) in Tokai-mura.

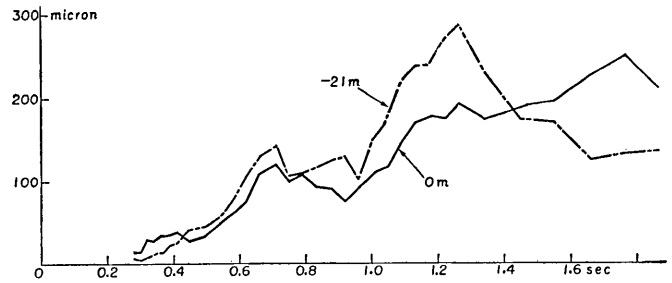

Fig. 41. Displacement spectra of earthquake No. 55 at place (A) in Tokai-mura.

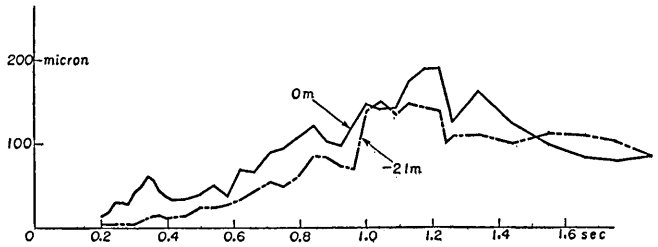

Fig. 42. Displacement spectra of earthquake No. 56 at place (A) in Tokai-mura.

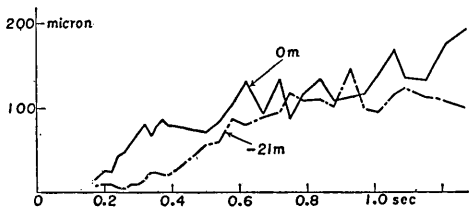

Fig. 43. Displacement spectra of earthquake No. 63 at place (A) in Tokai-mura.

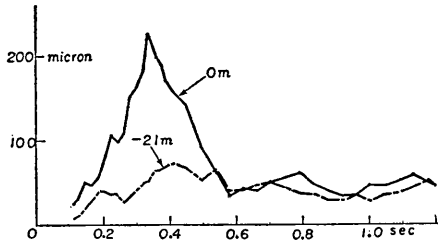

Fig. 44. Displacement spectra of earthquake No. 48 at place (A) in Tokai-mura.

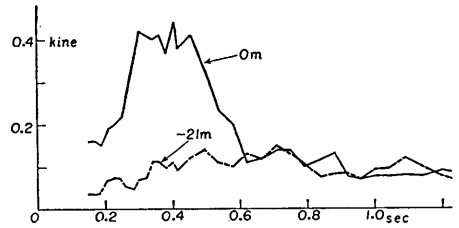

Fig. 45. Velocity spectra of earthquake No. 39 at place (A) in Tokai-mura.

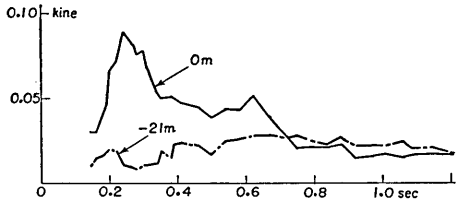

Fig. 46. Velocity spectra of earthquake No. 41 at place (A) in Tokai-mura.

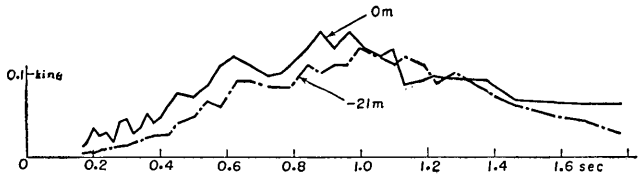

Fig. 47. Velocity spectra of earthquake No. 46 at place (A) in Tokai-mura.

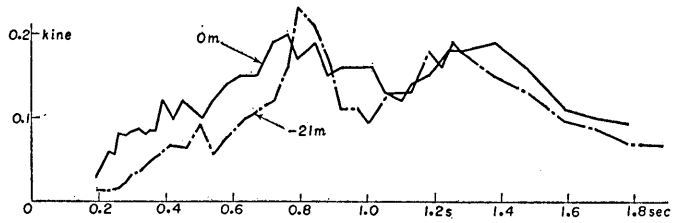

Fig. 48. Velocity spectra of earthquake No. 50 at place (A) in Tokai-mura.

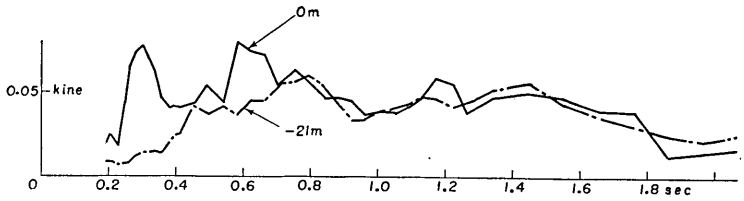

Fig. 49. Velocity spectra of earthquake No. 53 at place (A) in Tokai-mura.

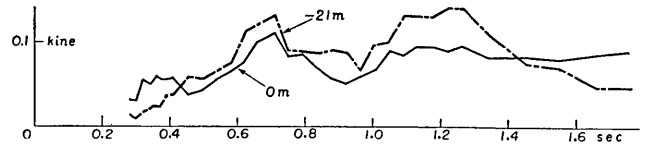

Fig. 50. Velocity spectra of earthquake No. 55 at place (A) in Tokai-mura.

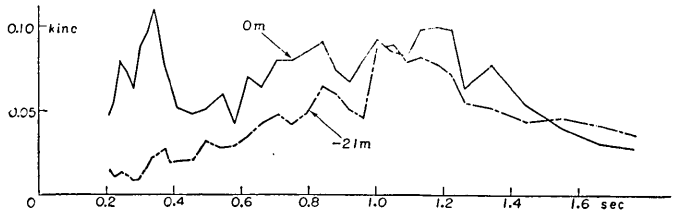

Fig. 51. Velocity spectra of earthquake No. 56 at place (A) in Tokai-mura.

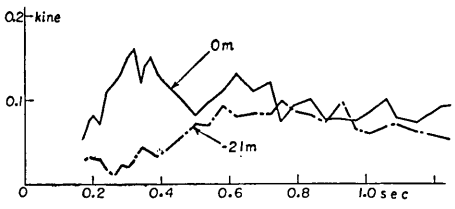

Fig. 52. Velocity spectra of earthquake No. 63 at place (A) in Tokai-mura.

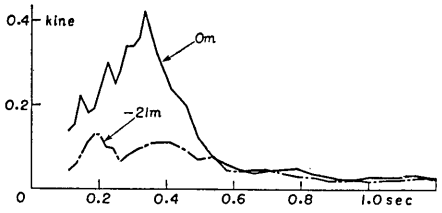

Fig. 53. Velocity spectra of earthquake No. 48 at place (A) in Tokai-mura.

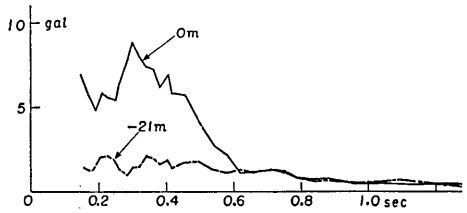

Fig. 54. Acceleration spectra of No. 39 earthquake at place (A) in Tokai-mura.

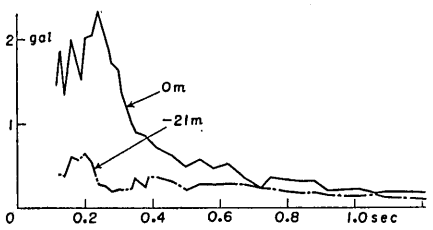

Fig. 55. Acceleration spectra of No. 41 earthquake at place (A) in Tokai-mura.

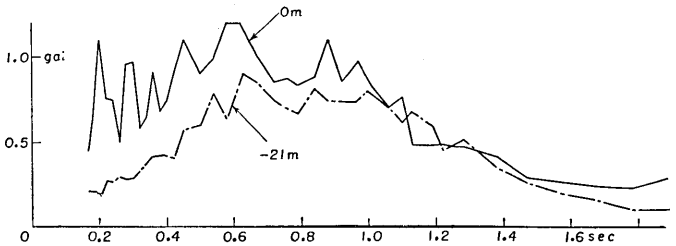

Fig. 56. Acceleration spectra of No. 46 earthquake at place (A) in Tokai-mura.

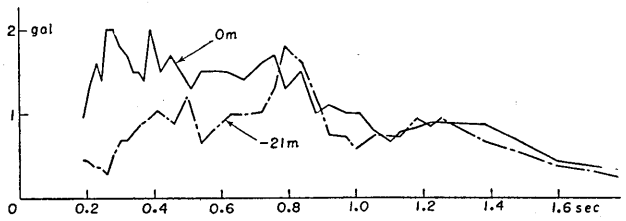

Fig. 57. Acceleration spectra of No. 50 earthquake at place (A) in Tokai-mura.

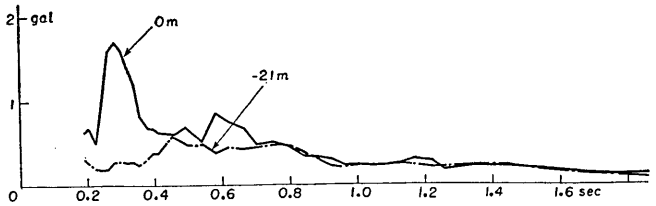

Fig. 58. Acceleration spectra of No. 53 earthquake at place (A) in Tokai-mura.

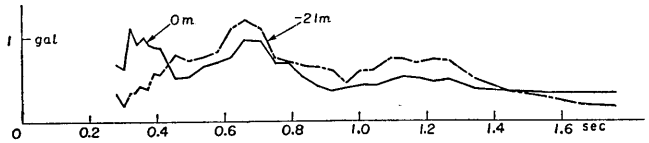

Fig. 59. Acceleration spectra of earthquake No. 55 at place (A) in Tokai-mura.

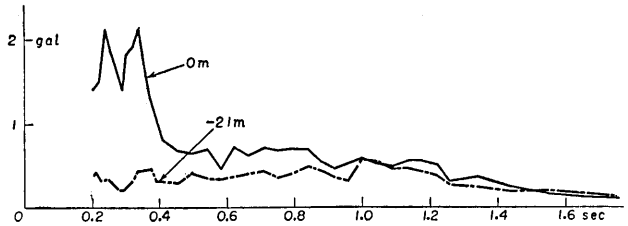

Fig. 60. Acceleration spectra of earthquake No. 56 at place (A) in Tokai-mura.

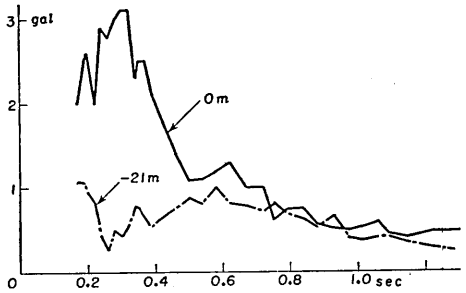

Fig. 61. Acceleration spectra of earthquake No. 63 at place (A) in Tokai-mura

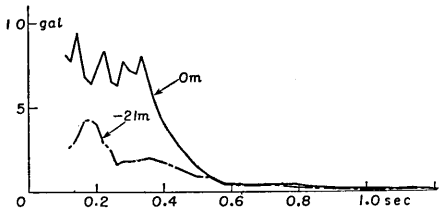

Fig. 62. Acceleration spectra of earthquake No. 48 at place (A) in Tokai-mura.

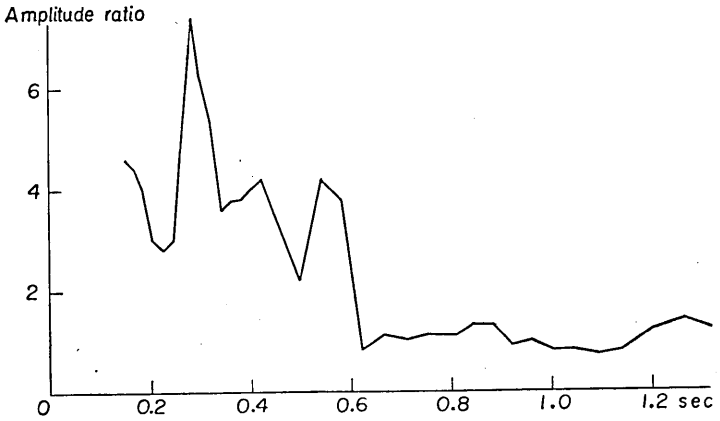

Fig. 63. The ratio of the amplitude on the ground to the one 21 m depth at place (A) in Tokai-mura. Earthquake number: 39.

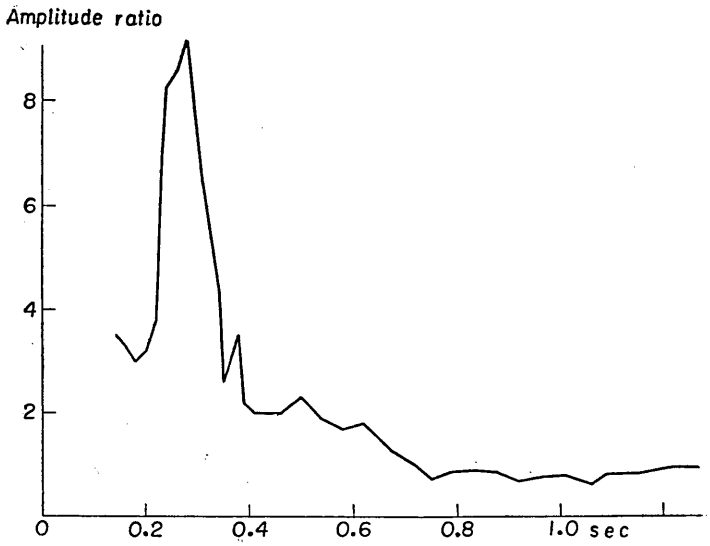

Fig. 64. The ratio of the amplitude on the ground to the one 21 m depth at place (A) in Tokai-mura. Earthquake number: 41.

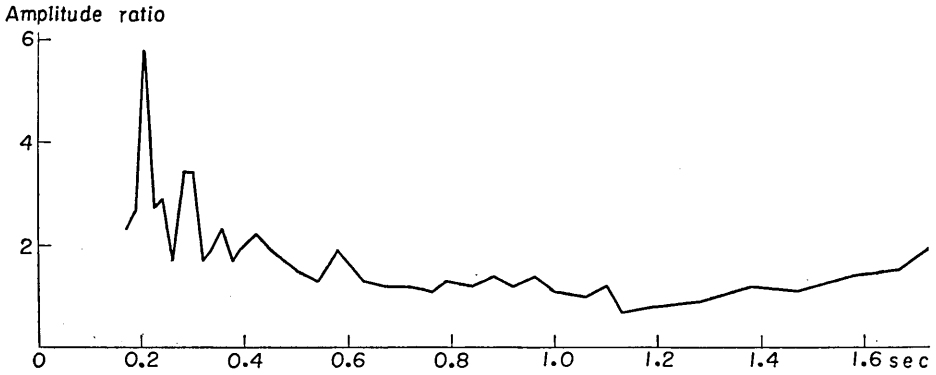

Fig. 65. The ratio of the amplitude on the ground to the one 21 m depth at place (A) in Tokai-mura. Earthquake number: 46.

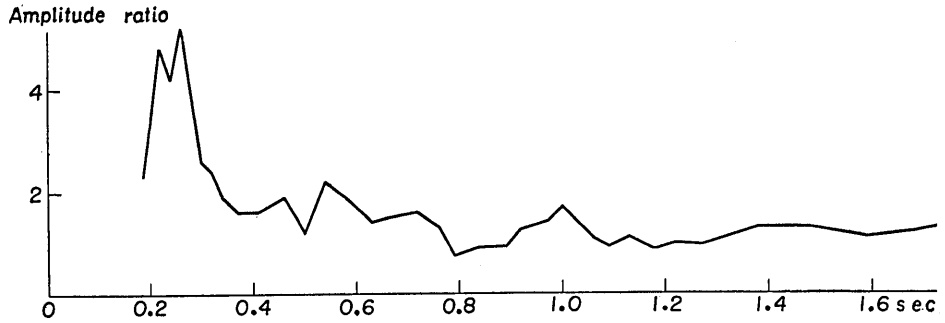

Fig. 66. The ratio of the amplitude on the ground to the one 21 m depth at place (A) in Tokai-mura. Earthquake number: 50.

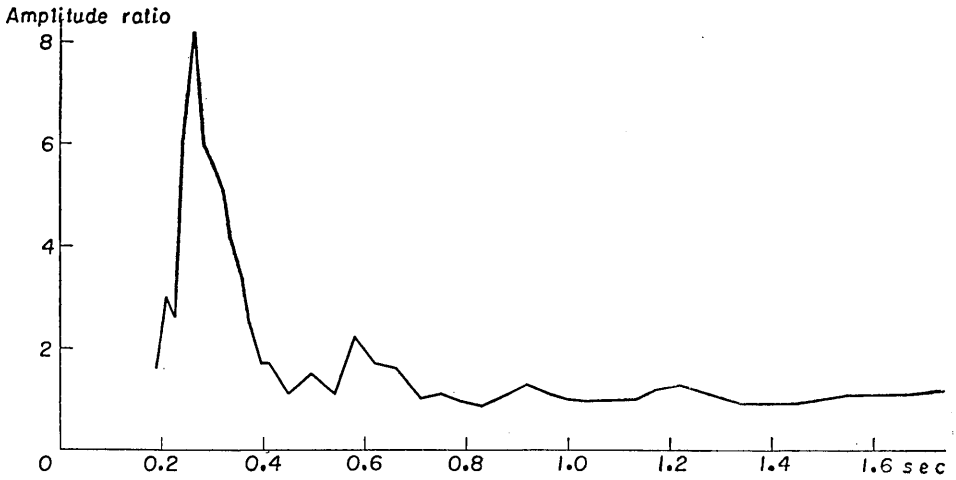

Fig. 67. The ratio of the amplitude on the ground to the one 21 m depth at place (A) in Tokai-mura. Earthquake number: 53.

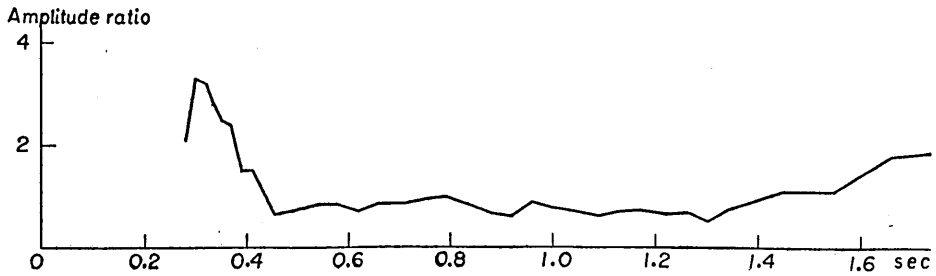

Fig. 68. The ratio of the amplitude on the ground to the one 21 m depth at place (A) in Tokai-mura. Earthquake number: 55.

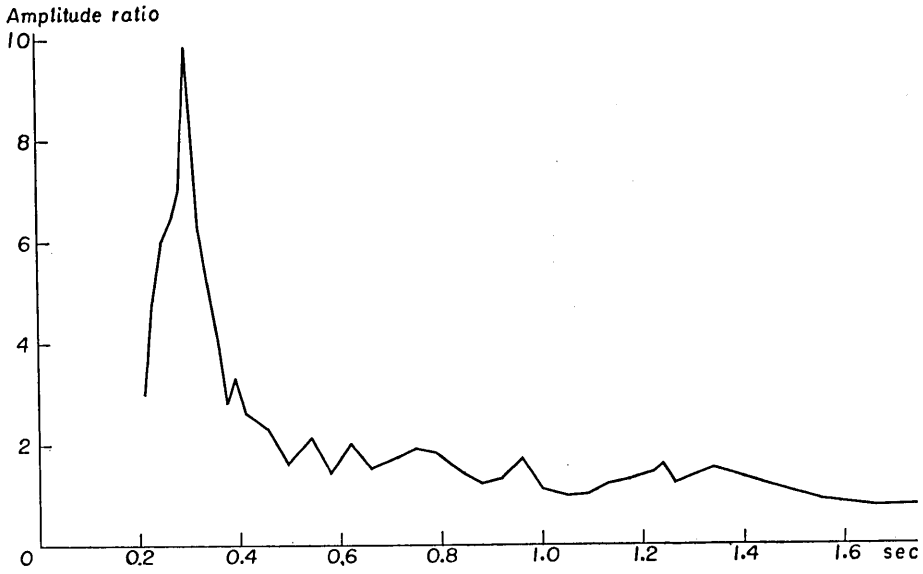

Fig. 69. The ratio of the amplitude on the ground to the one 21 m depth at place (A) in Tokai-mura. Earthquake number: 56.

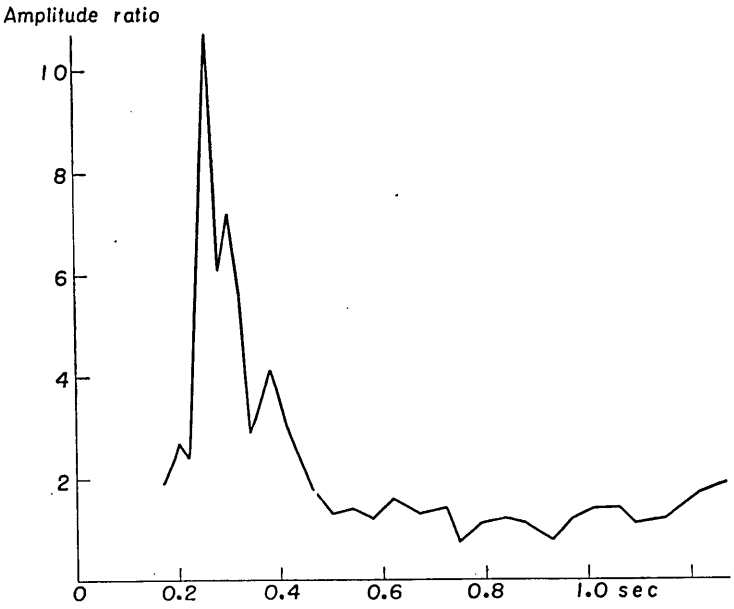

Fig. 70. The ratio of the amplitude on the ground to the one 21 m depth at place (A) in Tokai-mura. Earthquake number: 63.

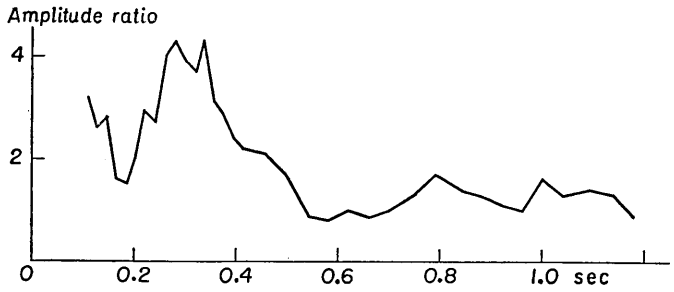

Fig. 71. The ratio of the amplitude on the ground to the one 21 m depth at place (A) in Tokai-mura. Earthquake number: 48.

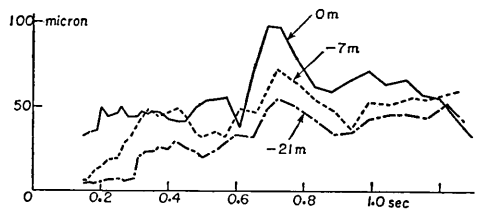

Fig. 72. Displacement spectra of earthquake No. 3 at place (B) in Tokai-mura.

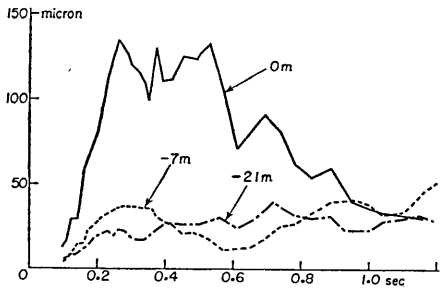

Fig. 73. Displacement spectra of earthquake No. 5 at place (B) in Tokai-mura.

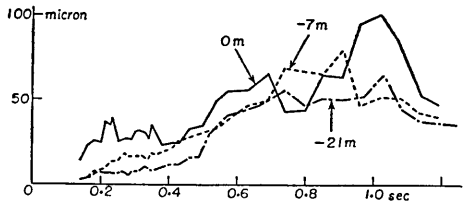

Fig. 74. Displacement spectra of earthquake No. 10 at place (B) in Tokai-mura.

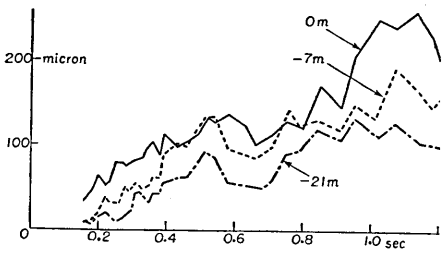

Fig. 75. Displacement spectra of earthquake No. 20 at place (B) in Tokai-mura.

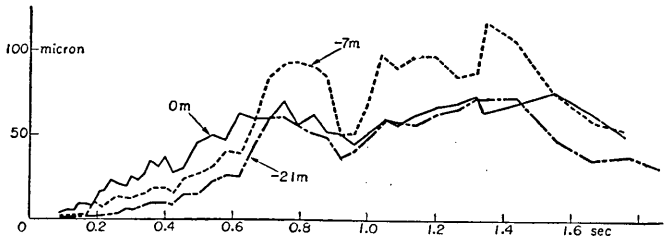

Fig. 76. Displacement spectra of earthquake No. 19 at place (B) in Tokai-mura.

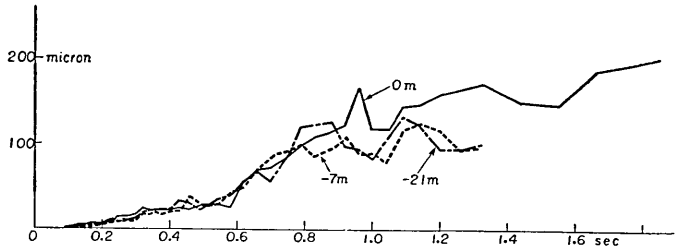

Fig. 77. Displacement spectra of earthquake No. 24 at place (B) in Tokai-mura.

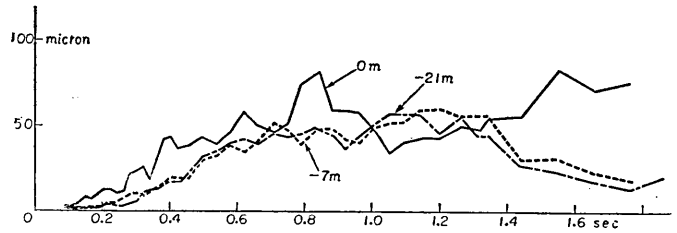

Fig. 78. Displacement spectra of earthquake No. 27 at place (B) in Tokai-mura.

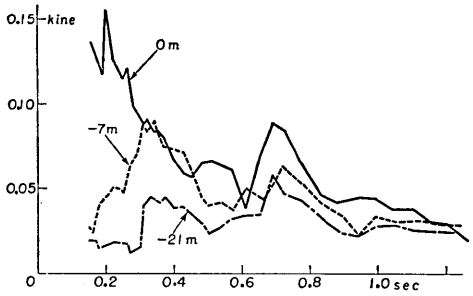

Fig. 79. Velocity spectra of earthquake No. 3 at place (B) in Tokai-mura.

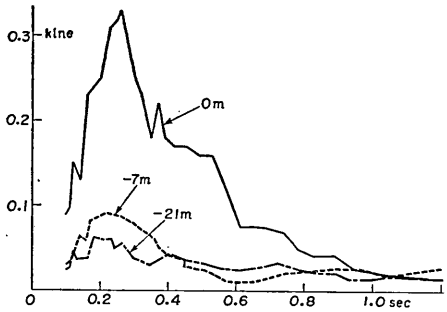

Fig. 80. Velocity spectra of earthquake No. 5 at place (B) in Tokai-mura.

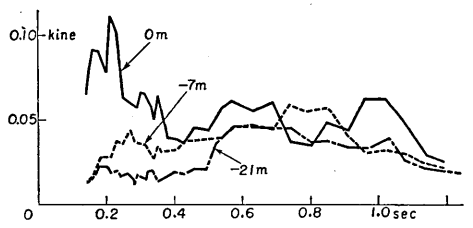

Fig. 81. Velocity spectra of earthquake No. 10 at place (B) in Tokai-mura.

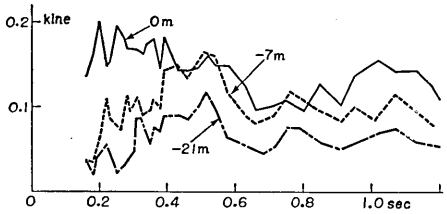

Fig. 82. Velocity spectra of earthquake No. 20 at place (B) in Tokai-mura.

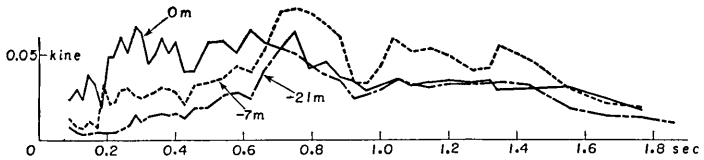

Fig. 83. Velocity spectra of earthquake No. 19 at place (B) in Tokai-mura.

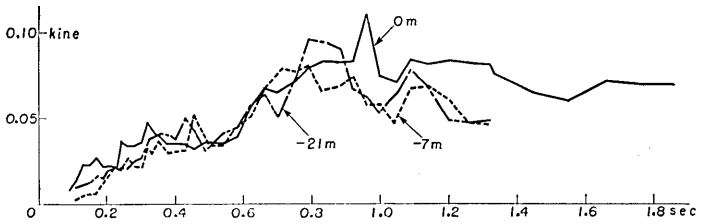

Fig. 84. Velocity spectra of earthquake No. 24 at place (B) in Tokai-mura.

Fig. 85. Velocity spectra of earthquake No. 27 at place (B) in Tokai-mura.

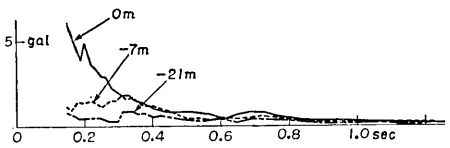

Fig. 86. Acceleration spectra of earthquake No. 3 at place (B) in Tokai-mura.

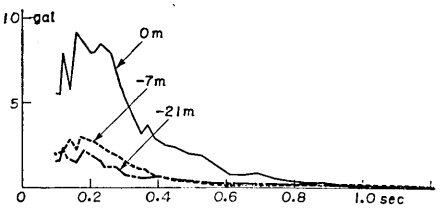

Fig. 87. Acceleration spectra of earthquake No. 5 at place (B) in Tokai-mura.

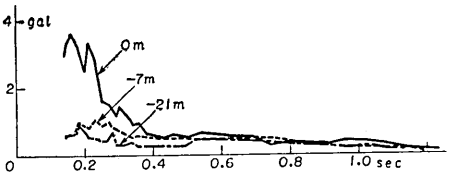

Fig. 88. Acceleration spectra of earthquake No. 10 at place (B) in Tokai-mura.

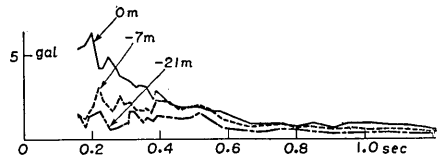

Fig. 89. Acceleration spectra of earthquake No. 20 at place (B) in Tokai-mura.

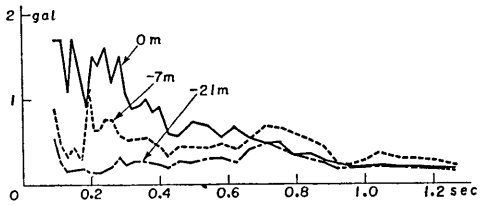

Fig. 90. Acceleration spectra of earthquake No. 19 at place (B) in Tokai-mura.

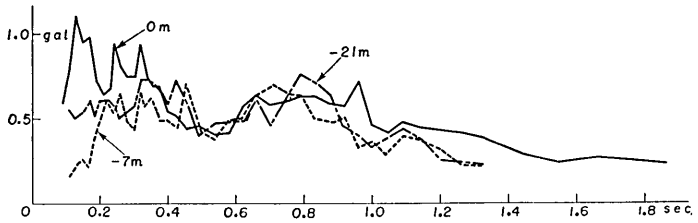

Fig. 91. Acceleration spectra of earthquake No. 24 at place (B) in Tokai-mura.

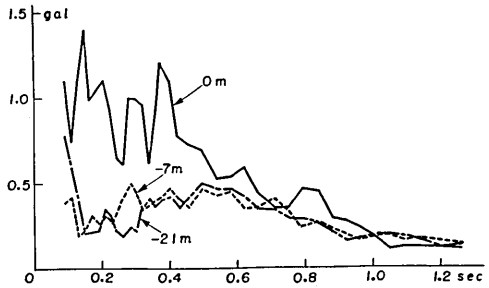

Fig. 92. Acceleration spectra of earthquake No. 27 at place (B) in Tokai-mura.

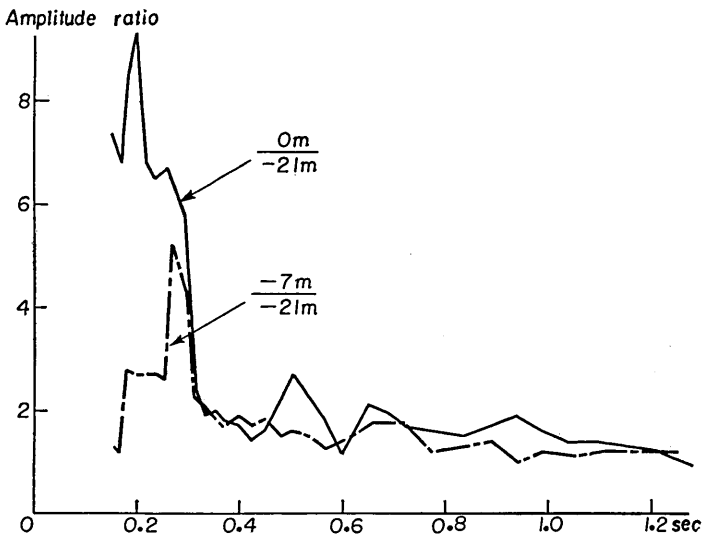

Fig. 93. Amplitude ratio corresponding to each period at place (B) in Tokai-mura. Earthquake number: 3.

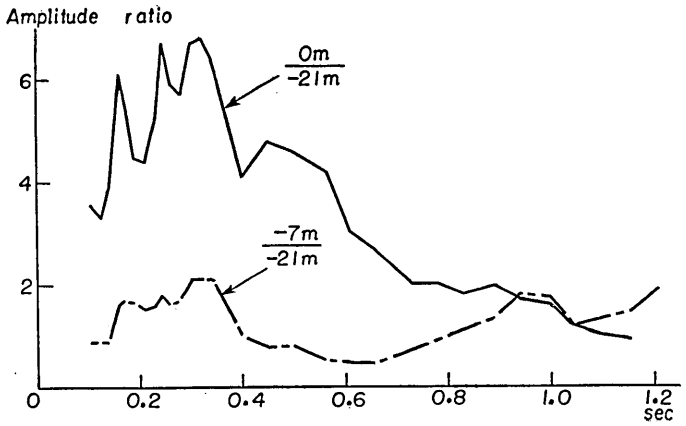

Fig. 94. Amplitude ratio corresponding to each period at place (B) in Tokai-mura. Earthquake number: 5.

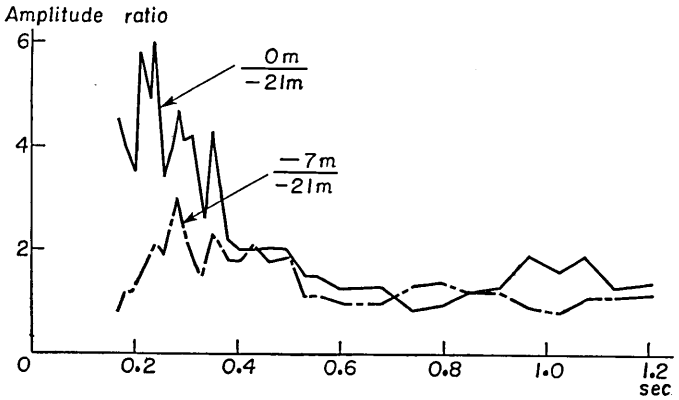

Fig. 95. Amplitude ratio corresponding to each period at place (B) in Tokai-mura. Earthquake number: 10.

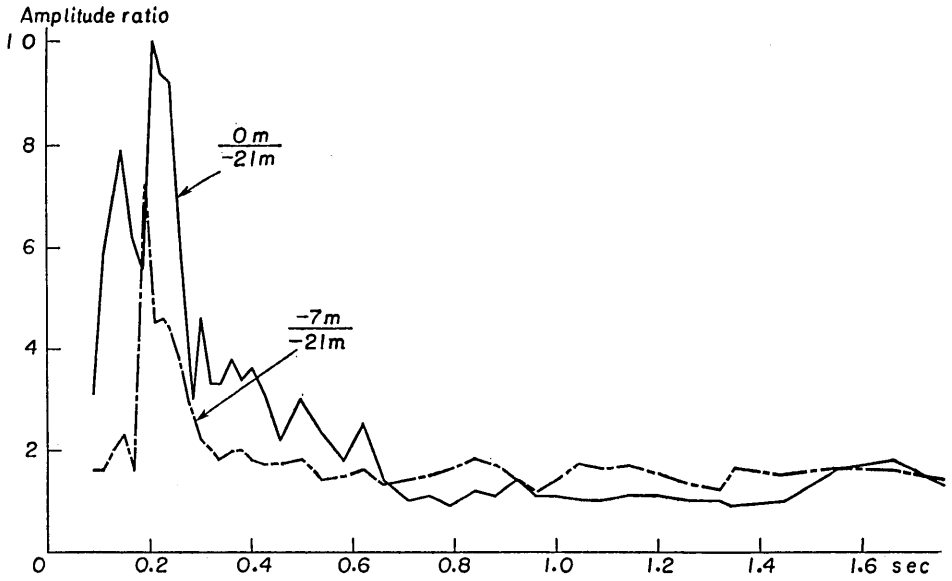

Fig. 96. Amplitude ratio corresponding to each period at place (B) in Tokai-mura. Earthquake number: 19.

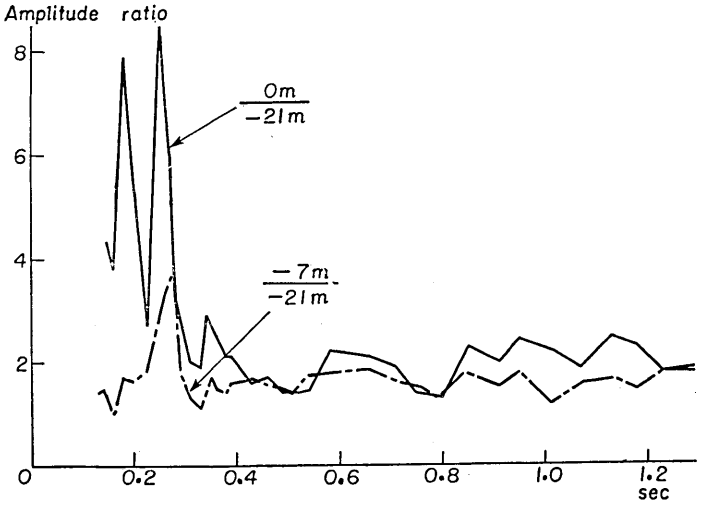

Fig. 97. Amplitude ratio corresponding to each period at place (B) in Tokai-mura. Earthquake number: 20.

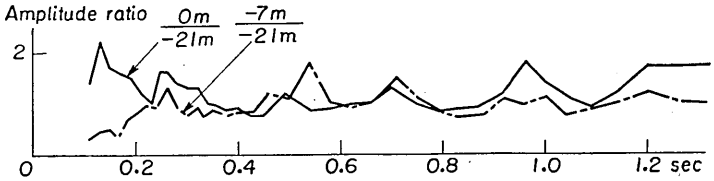

Fig. 98. Amplitude ratio corresponding to each period at place (B) in Tokai-mura. Earthquake number: 24.

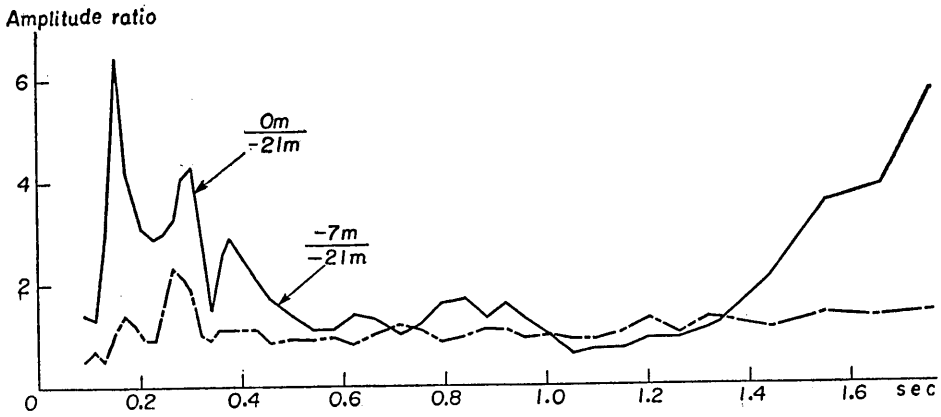

Fig. 99. Amplitude ratio corresponding to each period at place (B) in Tokai-mura. Earthquake number: 27.

4. Theoretical interpretation of the observational results

As mentioned in the former chapters, the curves of the relation between the amplitude ratio of earthquake motions on the ground to those underground and period seem to be similar to amplitude-period curve of a body having a single surface layer.

Here we shall examine the numerical calculations concerning the problem mentioned above, in which plane distortional waves propagated vertically upward in an elastic semi-infinite medium are partly transmitted and partly reflected at the bottom boundary of the superficial visco-elastic layer and are reflected at the free surface. This is one of the multiple reflection problems of elastic waves in a superficial layer.

Let the axis of z be drawn vertically downwards from the free surface of the layer of thickness H, and ρ_1, μ_1; ρ_2, μ_2 be density, elastic constants of both the surface layer and the lower medium, respectively, while, ξ_1 represent the viscous coefficient of the layer. T represents the period of waves. The equation of the ratio of the amplitude at the free surface, U, to the one of incident waves, u_0, obtained by one of the authors is as follows:[9]

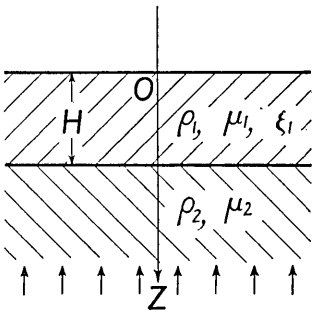

Fig. 100.

$$\frac{|U|}{|u_0|}=\frac{2}{\sqrt{\Phi_1^2+\Phi_2^2}} \tag{1}$$

in which

$$\left.\begin{aligned}\Phi_1&=\cos P\cosh Q+\alpha(R\cos P\sinh Q-S\sin P\cosh Q)\,,\\ \Phi_2&=\sin P\sinh Q+\alpha(R\sin P\cosh Q+S\cos P\sinh Q)\,,\end{aligned}\right\} \tag{2}$$

in (2)

$$\left.\begin{aligned}&P=\frac{\pi T_0}{2T}M\cos(N)\,, && Q=\frac{\pi T_0}{2T}M\sin(N)\,,\\ &R=M\left\{\cos(N)+\frac{\tau}{T}\sin(N)\right\}\,, && S=M\left\{\frac{\tau}{T}\cos(N)-\sin(N)\right\}\,,\\ &\alpha=\frac{v_1\rho_1}{v_2\rho_2}\,, && T_0=\frac{4H}{v_1}\end{aligned}\right\} \tag{3}$$

9) K. KANAI, *Bull. Earthq. Res. Inst.*, **28** (1950), 31-35.

in (3)

$$M=\left\{1+\left(\frac{\tau}{T}\right)^2\right\}^{-1/4}, \qquad N=\frac{1}{2}\tan^{-1}\left(\frac{\tau}{T}\right), \qquad \tau=\frac{2\pi\xi_1}{\mu_1} \qquad (4)$$

The average curves of the amplitude ratio of the ground surface to the underground at Hitachi Mine, and at places (A) and (B) in Tokai-mura are shown in Figs. 101, 102 and 103, respectively by full lines. Fig. 104 represents the amplitude ratio at two spots of different depth at place (B) in Tokai-mura.

(i) The case of Hitachi Mine.

Now, we adopt 132 m/s[10] as v_1 and the predominant period of the ground obtained from the frequency analysis of micro-tremor, 0.18 sec, as T_0. The value of $v_2=1730$ m/s is estimated from the velocity of P-waves of 3,000 m/s[11] and the assumption of Poisson's ratio=1/4. Assuming $\rho_1=\rho_2$, we obtain the value of $\alpha=1/13$ as ρ_1v_1/ρ_2v_2. Substituting the values of $\alpha=1/13$ and $T_0=0.18$ sec in equations (1)~(4), the theoretical spectral response curve, which coincides mostly with the observational result as shown in Fig. 101 by full line, can be obtained through the trial and error method by changing the value of τ.

The value of τ used finally is $\tau=0.034$, that is, $\xi_1/\mu_1=5.4\times10^{-3}$ sec^{-1} and the calculated result mentioned above is shown in Fig. 101 by broken line.

(ii) The case of place (A) in Tokai-mura.

The predominant period of the ground obtained from the frequency analysis of micro-tremor, 0.27 sec, is adopted as T_0.

The value of $v_1=112$ m/s is estimated from the relations of $v_1=4H/T_0$ and $H=7.55$ m, which is thickness of the sand layer (see Fig. 33).

The value of $v_2=920$ m/s is estimated from the velocity of P-waves of 1,600 m/s[12] and the assumption of Poisson's ratio=1/4. Assuming $\rho_1=\rho_2$, we obtain the value of $\alpha=1/8.2$ as ρ_1v_1/ρ_2v_2.

Substituting the values of $\alpha=1/8.2$ and $T_0=0.27$ sec in equations (1)~(4) and carrying out the trial and error method, we obtained the theoretical spectral sesponse curve, which coincides mostly with the observational result as shown in Fig. 102 by a full line. (In this case, the numerator of equation (1) takes 1 without 2, because, the observation value at -21 m is considered twice of the value of the incident waves.) The value of τ used finally is $\tau=0.020$, that is, $\xi_1/\mu_1=3.2\times10^{-3}$ sec^{-1} and

10) K. KANAI, T. TANAKA and T. SUZUKI, *Bull. Earthq. Res. Inst.*, **36** (1958), 215.
11) K. KANAI, *Bull. Earthq. Res. Inst.*, **29** (1951), 506, Fig. 4.
12) S. OMOTE, *Monthly Meeting of the Earthquake Research Institute*, (Feb. 1957).

the calculated result mentioned above is shown in Fig. 102 by broken line.

(iii) The case of place (B) in Tokai-mura.

In this case, the predominant period of the ground obtained from the frequency analysis of micro-tremor, 0.24 sec, is adopted as T_0. The value of $v_1=117$ m/s is estimated from the relations of $v_1=4H/T_0$ and $H=7$ m, which is thickness of the sand layer (see Fig. 33). The value of $v_2=920$ m/s is the same as the case of place (A). Assuming $\rho_1=\rho_2$, we obtain the value of $\alpha=1/7.9$ as $\rho_1 v_1/\rho_2 v_2$.

Substituting the values of $\alpha=1/7.9$ and $T_0=0.24$ sec in equations (1)~(4) and using the trial and error method, too, we obtained the theoretical spectral response curve, which is coincident mostly with the observational result as shown in Fig. 103 by full line. (In this case, the numerator of equation (1) takes 1 without 2, because the observation value at -21 m is considered twice of the value of the incident waves.) The value of τ used finally is $\tau=0.017$, that is, $\xi_1/\mu_1=2.7\times10^{-3}$ sec^{-1} and the calculated result mentioned above is shown in Fig. 103 by broken line.

Figs. 101~103 tell us a noteworthy result that the amplitude on the ground grows very large depending on the multiple reflection of seismic waves in the superficial layer, as the values of $\xi_1/\mu_1=(3\sim5)\times10^{-3}$

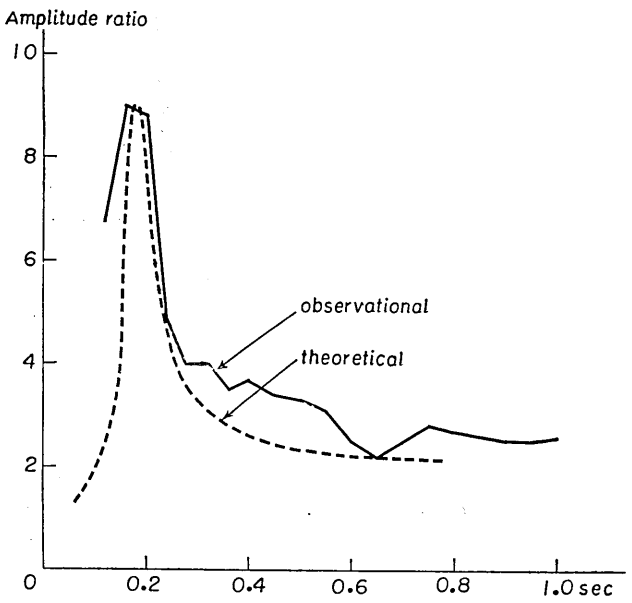

Fig. 101. Average amplitude ratio of 0 m to -300 m at Hitachi Mine.

sec^{-1} are plausible and the observational and calculated results coincide considerably well with each other.

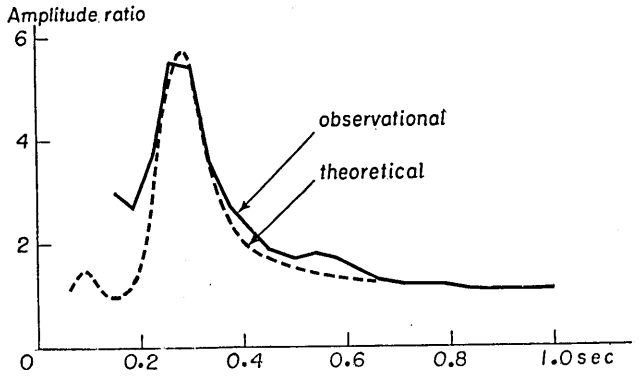

Fig. 102. Average amplitude ratio of 0 m to −21 m at place (A) in Tokai-mura.

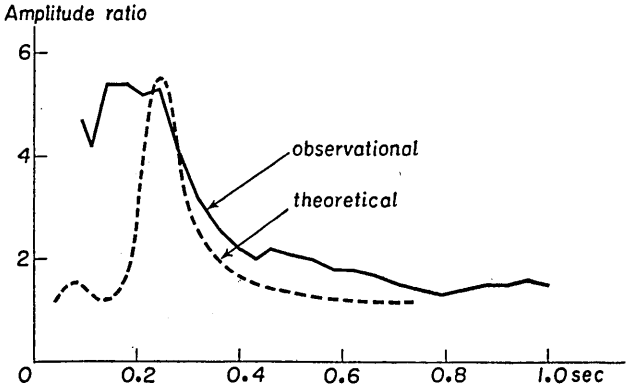

Fig. 103. Average amplitude ratio of 0 m to −21 m at place (B) in Tokai-mura.

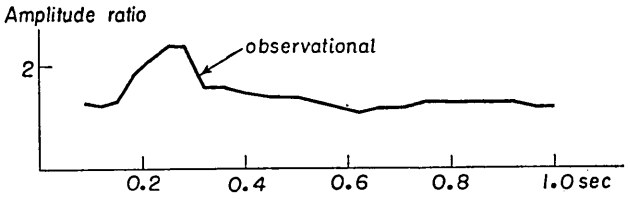

Fig. 104. Average amplitude ratio of −7 m to −21 m at place (B) in Tokai-mura.

5. Acknowledgement

In conclusion, we wish to express our thanks to Motoyama-office, Hitachi Mine and Japan Atomic Power Research Institute for their co-operation in the course of these investigations, and also to Messrs. T. Suzuki and K. Osada without whose help this work could not be done.

---

5. 地下における地震動の研究
(重複反射の問題)

地震研究所 { 金井　清 / 田中貞二 / 吉沢静代 }

この研究は，茨城県日立鉱山の地上と地下 300 m，茨城県東海村（日本原子力研究所構内）の地上と地下 21 m (場所 (A))，地上と地下 7 m，21 m (場所 (B)) の 3 組の地震動比較観測を行い，その記録をレスポンス，コンピューターによつて周期解析したものである．次に，この研究でわかつたことを列挙する．

（1） 地下深所における地震動の変位スペクトラムには山があり，その山になる周期は地震が大きいほど長くなる．

（2） 変位スペクトムラの極大になる周期よりも長い周期のものと，0.1 秒位よりも短い周期のものとをのぞくと，各周期の波についての速度は，ほぼ一定である．即ち勢力の等分配の法則が大体成り立つ．

（3） 地下に対する地上の地震動のスペクトラムの比をとると，或周期で，非常にはつきりした山ができる．その山になる周期は各場所特有の値となり，この値は地盤の固有周期に相当する．

（4） 加速度スペクトラムの山になる周期は，上述の周期と一致する．

（5） 東海村の地下 7 m と地下 21 m のスペクトラム比には，わずかな山ができ，この山の周期は前述の周期と一致する．

（6） 地下対地上スペクトラム比の曲線は，1 層からなる地表層内での弾性波の重複反射現象で，相当よく説明される．

（7） 上述の数理計算を実測値に合わせて得られた，表面層の物質の粘性係数 ξ と剛性率 μ の比は $\xi/\mu=0.02\ \mathrm{sec}^{-1}$ で，他の研究から求められた値と矛盾しない．

（8） 地下対地上スペクトラムの山になる周期は地上における常時微動の頻度の山になる周期とよく合う．

（9） この観測には，新作の，自動水準式地震計並びに地震計用スターターを使つたが，これらの計器は所期の成績をおさめた．
